# Determination of Shale Volume and Distribution Patterns and Effective Porosity from Well Log Data Based On Cross-Plot Approach for A Shaly Carbonate Gas Reservoir

**Siyamak Moradi [1], Mohammad Moeini [1], Mohammad Kamal Ghassem al-Askari [2], Elaheh Hamed Mahvelati [1]**

[1] Abadan Faculty of Petroleum Engineering, Petroleum University of Technology, Abadan, Iran
[2] Ahwaz Faculty of Petroleum Engineering, Petroleum University of Technology, Ahwaz, Iran

E-mail address: moradi.s@put.ac.ir

**Abstract**. Determination of shale volume distribution is one of the most important factors that has to be considered in formation evaluation, since existence of shale reduces effective porosity and permeability of the reservoir. In this paper, shale volume and distribution (dispersed, laminar and structural) and formation effective porosity are estimated from well log data and cross-plots. Results show that distribution of shale is mainly dispersed with few of laminar ones, and the quality of reservoir (effective porosity) decreases with depth resulting in low productivity of gas wells drilled in lower zones. Good agreement of estimated shale volumes and effective porosities from neutron-density cross-plot with the values determined from gamma ray log (CGR) and core analysis demonstrates the accuracy and applicability of these plots in determination of petrophysical parameters from conventional log data.

## 1. Introduction

Shale is a clay-rich heterogeneous rock which contains variable content of clay minerals (mostly illite, kaolinite, chlorite and montmorillonite) and organic matter [1, 2]. Presence of shale in the formation has sever effects on petrophysical properties and reduces effective and total porosity and permeability of the reservoir [3, 4]. Moreover, existence of shale causes uncertainties in formation evaluation and proper estimation of oil and gas reserves [5].

Shale distribution influences the evaluation of all principal reservoir characteristics e.g. effective porosity, water saturation, and permeability [6, 7]. Dispersed shale is composed of clay particles, fragments or crystals to be found on grain surface that occupy void spaces between matrix particles and reduce the effective porosity ($\varphi_e$) and permeability significantly [8]. Structural shale exists in the form of fragments or crystals which are an integral part of the rock framework and is considered as a portion of rock matrix [9]. Laminar shale exists as layer of shale which does not exceed 0.5 in. (1.27 cm) thickness within clean formations. The effect of two last shale types on porosity and permeability is assumed to be negligible [2, 10]. In this paper, shale volume and distribution type, and effective porosity of the formation are determined from well log data depicted on triangle density-neutron porosity cross-plots which are introduced as a quick and accurate method in determination of rock petrophysical parameters [11].

## 2. Methodology

A triangle neutron-density porosity ($\varphi_N$ Vs. $\varphi_D$) cross-plot is used to determine shale type and volume, and effective porosity (Fig. 1). Three distinct points (***F, M, Sh***) are shown in this cross-plot; Point ***F*** represents fluid or water point where $\varphi_D = \varphi_N = 100\%$. Point ***M*** represents matrix point; if density and neutron tools are calibrated in terms of the existing matrix, then $\varphi_N = \varphi_D = 0$. Point ***SH*** represents shale point; the coordinate of point ***SH*** [$\varphi_{NSh}$ , $\varphi_{DSh}$] must be determined for shaliest portion of well and this coordinate varies from well to well and has to be estimated for each case.

Data points representing $\varphi_N$ and $\varphi_D$ values in clean formations (i.e $V_{sh}=0$) fall on ***M-F*** line and their position on the line indicates effective porosity values. Line ***M-Sh*** represents $\varphi_e=0$ line and value of each point on this line indicates shale volume of the formation with zero effective porosity. Because of porosity values do not exceed 50%, line ***M-F*** is plotted till 50% porosity to make full use of cross-plot ([12, 13]. The following equations are used to construct this triangle cross-plot [13]:

$$\begin{cases} \boldsymbol{\varphi_e} = \boldsymbol{\varphi_N} - (\boldsymbol{\varphi_{NSH}} \cdot \boldsymbol{V_{SH}}) \\ \boldsymbol{\varphi_e} = \boldsymbol{\varphi_D} - (\boldsymbol{\varphi_{DSH}} \cdot \boldsymbol{V_{SH}}) \end{cases} \quad (1)$$

The laminar, dispersed and structural shale points areas fall on or around ***LS-Sh, DIS*** and ***STR*** lines, respectively. For each point within triangle $V_{Sh}$ is estimated on ***M-Sh*** line parallel to clean formation line, and also, $\varphi_e$ is determined on clean formation line parallel to ***M-Sh*** line. For example, point ***A*** in Fig. 1 represents a shaly formation that has values of $\varphi_e$ = 9% and $V_{Sh}$ = 23% with dispersed shale content.

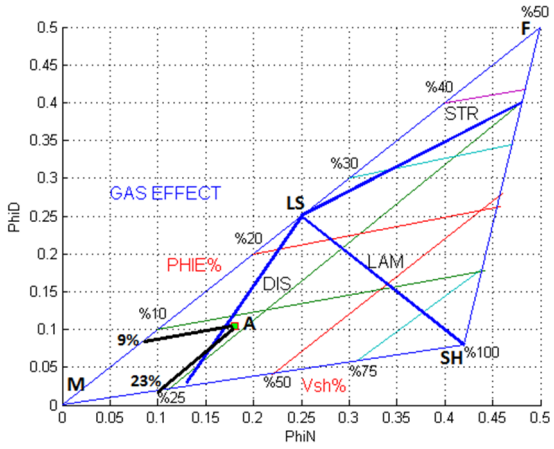


**Figure 1.** Triangle neutron-density porosity cross-plot

*2.1 Gas correction for neutron porosity*

If formation contains hydrocarbons, neutron and density porosities have to be corrected before points are plotted since calculated shale volumes will be too low in gas-bearing intervals [14, 15]. The procedure of hydrocarbon correction is as follows [1].

$$\boldsymbol{\varphi_{Ncorr}} = \boldsymbol{\varphi_N} - \boldsymbol{\Delta\varphi_N} \quad \text{where} \quad \boldsymbol{\Delta\varphi_N} = \boldsymbol{\varphi} \times \boldsymbol{S_{hr}} \frac{2.2\rho_h - 1.0 + 0.4P}{1 - 0.4P} \quad (2)$$

$$\boldsymbol{\varphi_{dcorr}} = \boldsymbol{\varphi_d} - \boldsymbol{\Delta\varphi_d} \quad \text{where} \quad \boldsymbol{\Delta\varphi_d} = 1.07\boldsymbol{\varphi} \times \boldsymbol{S_{hr}} \frac{(1.11(1-\rho_h) + 0.65P - 0.03)}{\rho_{ma} - 1.0 - 0.7P} \quad (3)$$

where ***P*** is salinity of the mud (PPM×10), $\boldsymbol{\varphi_N}$ is neutron porosity, $\boldsymbol{\varphi_{Ncorr}}$ and $\boldsymbol{\varphi_{dcorr}}$ are corrected neutron and density porosities, $\boldsymbol{\rho_h}$ is hydrocarbon density and $\boldsymbol{S_{hr}}$ is residual hydrocarbon saturation. Hydrocarbon density $\rho_h$ can be estimated by:

$$\rho_h = \frac{\left(1+0.72\frac{\varphi_N}{\varphi_d}\right)S_{hr}-\left(1-\frac{\varphi_N}{\varphi_d}\right)}{\left(2.2+0.8\frac{\varphi_N}{\varphi_d}\right)S_{hr}} \quad (4)$$

Residual gas saturation is used since neutron and density tools investigate the flushed zone. The portion of hydrocarbon in the invaded zone is given by Archie's equation [15]:

$$S_{xo} = \sqrt{\left(\frac{a}{\varphi^m} \times \frac{R_{mf}}{R_{xo}}\right)} = \sqrt{\frac{FR_{mf}}{R_{xo}}} \quad (5)$$

where $\varphi$ is porosity, $m$ is cementation factor, $a$ is formula constant, $R_{mf}$ is resistivity of mud filtrate and $R_{xo}$ is resistivity of flushed zone and residual gas saturation is $S_{hr} = 1 - S_{xo}$.
In this study, $V_{sh}$ estimated from cross-plot method is validated with $V_{sh}$ calculated from gamma ray log (CGR). The following equations are used to determine shale volume:

$$I_{GR} = \frac{GR_{log}-GR_{min}}{GR_{max}-GR_{min}} \quad (6)$$

where $\mathbf{I_{GR}}$ is the gamma ray index, $\mathbf{GR_{log}}$ is the gamma ray response in the zone of interest, $\mathbf{GR_{min}}$ is the gamma ray response in cleanest formation, $\mathbf{GR_{max}}$ is the gamma ray response in shale layer. The shale volume ($V_{sh}$) can be calculated from the gamma ray index [17]:

$$V_{Sh} = \frac{I_{GR}}{3-2\,I_{GR}} \quad (7)$$

## 3. Results and Discussions

The studied formation is a lower Triassic sequence composed of eolithic calcite with few of anhydrite and secondary dolomite. Five depth intervals are selected so that different shale volumes exist in each part in order to extend the working criteria to a wide range of shaliness. The coordinate of shale point is determined from well logs to be $\varphi_{Nsh}$ = 42% and $\varphi_{Dsh}$ = 8%. Cross-plots for studied intervals are shown in Figures 2-7.

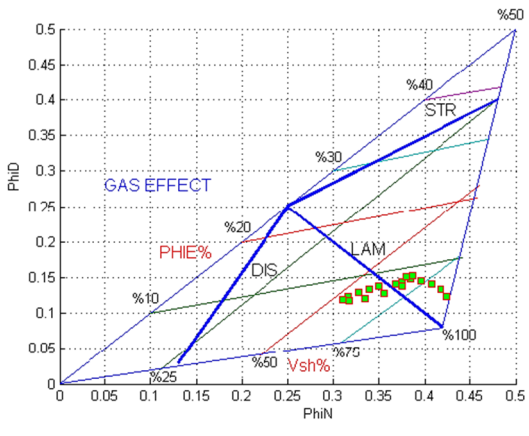


**Figure 2.** Depth interval 2590-2592m (aggregation of points is around laminar shale line)

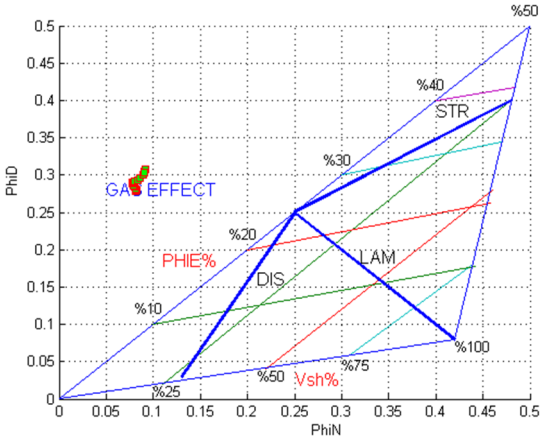


**Figure 3.** Depth interval 2650.3-2652m (before hydrocarbon correction)

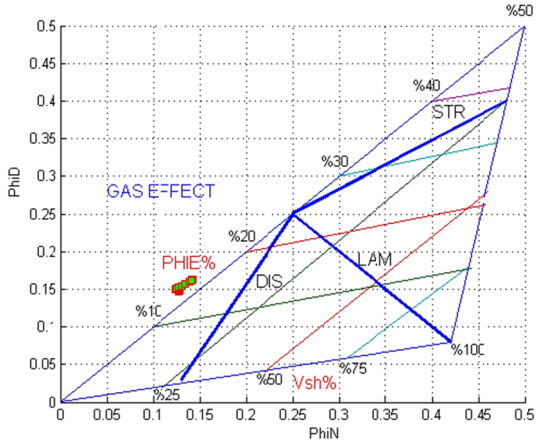


**Fig. 4.** Depth interval 2650.3-2652m (after hydrocarbon correction-no shale)

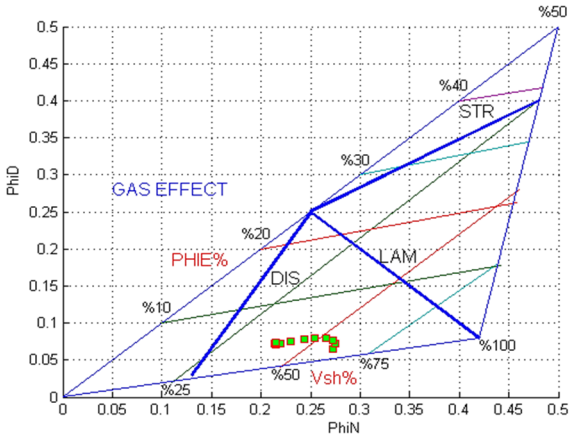


**Fig. 5.** Depth interval 2718.5-2719.5m (combination of laminar and dispersed shales)

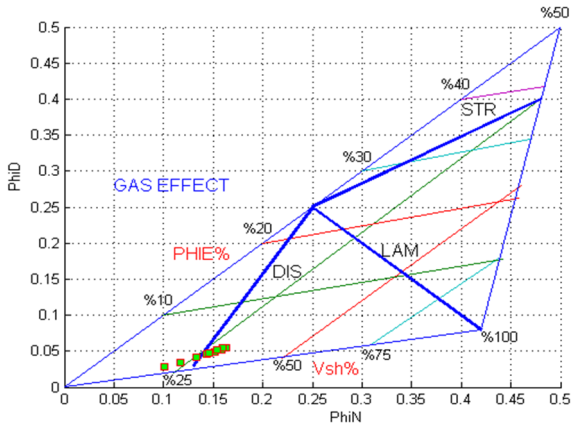


**Fig. 6.** Depth interval 2730.5-2731.5m (dispersed shale)

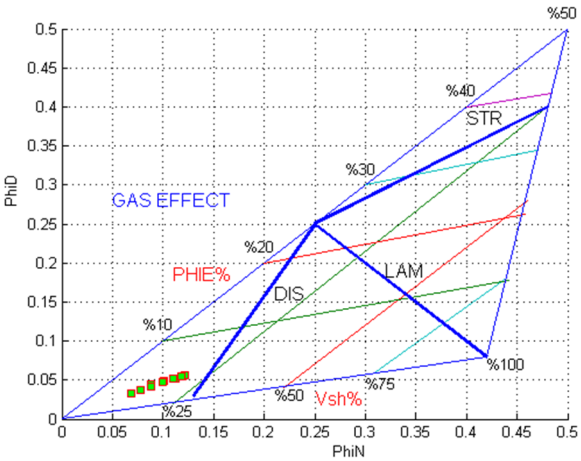


**Fig. 7.** Depth interval 2743.-2744m (dispersed shale)

Raw data of neutron and density logs (PHI-N, PHI-D) and estimated shale volumes and effective porosities (PHIE) from cross-plot (VSH-CP) and gamma ray log (VSH-GR) for mentioned intervals are also presented in Tables 1-5.

**Table 1.** $V_{sh}$ and $\varphi_e$ estimates for depth interval of 2590-2592 m

| PHI-N | PHI-D | PHIE-CP % | VSH-CP | PHI-N | PHI-D | PHIE-CP % | VSH-CP |
|---|---|---|---|---|---|---|---|
| 0.424 | 0.122 | 0.051 | 0.88 | 0.315 | 0.123 | 0.087 | 0.56 |
| 0.417 | 0.133 | 0.067 | 0.83 | 0.309 | 0.119 | 0.074 | 0.56 |
| 0.407 | 0.141 | 0.079 | 0.78 | 0.317 | 0.117 | 0.070 | 0.58 |
| 0.395 | 0.145 | 0.085 | 0.73 | 0.335 | 0.120 | 0.069 | 0.63 |
| 0.375 | 0.144 | 0.090 | 0.67 | 0.355 | 0.127 | 0.074 | 0.67 |
| 0.367 | 0.141 | 0.088 | 0.66 | 0.374 | 0.138 | 0.082 | 0.69 |
| 0.350 | 0.137 | 0.088 | 0.62 | 0.384 | 0.148 | 0.092 | 0.69 |
| 0.339 | 0.133 | 0.085 | 0.60 | 0.387 | 0.153 | 0.098 | 0.68 |

**Table 2.** $V_{sh}$ and $\varphi_e$ estimated from cross-plot for 2650.3-2652m depth interval

| PHI-N | PHI-D | PHIE | VSH-CP | VSH-GR | PHI-N | PHI-D | PHIE | VSH-CP | VSH-GR |
|---|---|---|---|---|---|---|---|---|---|
| 0.127 | 0.147 | 0.152 | 0 | 0 | 0.124 | 0.150 | 0.156 | 0 | 0 |
| 0.127 | 0.148 | 0.152 | 0 | 0 | 0.125 | 0.151 | 0.157 | 0 | 0 |
| 0.128 | 0.148 | 0.153 | 0 | 0 | 0.127 | 0.152 | 0.158 | 0 | 0 |
| 0.127 | 0.149 | 0.153 | 0 | 0 | 0.130 | 0.153 | 0.159 | 0 | 0 |
| 0.126 | 0.149 | 0.154 | 0 | 0 | 0.134 | 0.156 | 0.161 | 0 | 0 |
| 0.125 | 0.150 | 0.155 | 0 | 0 | 0.138 | 0.159 | 0.164 | 0 | 0 |
| 0.124 | 0.150 | 0. 156 | 0 | 0 | | | | | |

**Table 3.** $V_{sh}$ and $\varphi_e$ estimated from cross-plot for 2718.5-2719.5m depth interval

| PHI-N | PHI-D | PHIE | VSH-CP | VSH-GR | PHI-N | PHI-D | PHIE | VSH-CP | VSH-GR |
|---|---|---|---|---|---|---|---|---|---|
| 0.272 | 0.065 | 0.017 | 0.607 | 0.557 | 0.230 | 0.074 | 0.038 | 0.458 | 0.411 |
| 0.274 | 0.072 | 0.024 | 0.595 | 0.604 | 0.219 | 0.071 | 0.037 | 0.434 | 0.376 |
| 0.272 | 0.077 | 0.031 | 0.574 | 0.620 | 0.214 | 0.071 | 0.037 | 0.422 | 0.363 |
| 0.264 | 0.079 | 0.036 | 0.545 | 0.593 | 0.214 | 0.072 | 0.038 | 0.418 | 0.368 |
| 0.254 | 0.079 | 0.038 | 0.513 | 0.534 | 0.215 | 0.074 | 0.040 | 0.414 | 0.384 |
| 0.244 | 0.077 | 0.038 | 0.489 | 0.466 | | | | | |

**Table 4.** $V_{sh}$ and $\varphi_e$ estimated from cross-plot for 2730.5-2731.5m depth interval

| PHI-N | PHI-D | PHIE | VSH-CP | VSH-GR | PHI-N | PHI-D | PHIE | VSH-CP | VSH-GR |
|---|---|---|---|---|---|---|---|---|---|
| 0.142 | 0.045 | 0.022 | 0.286 | 0.207 | 0.159 | 0.054 | 0.029 | 0.310 | 0.272 |
| 0.151 | 0.049 | 0.024 | 0.302 | 0.239 | 0.154 | 0.051 | 0.027 | 0.301 | 0.247 |
| 0.158 | 0.052 | 0.027 | 0.312 | 0.270 | 0.145 | 0.047 | 0.024 | 0.288 | 0.224 |
| 0.162 | 0.054 | 0.028 | 0.319 | 0.289 | 0.132 | 0.041 | 0.019 | 0.270 | 0.205 |
| 0.163 | 0.055 | 0.029 | 0.318 | 0.289 | 0.117 | 0.034 | 0.014 | 0.243 | 0.190 |

**Table.5** $V_{sh}$ and $\varphi_e$ estimated from cross-plot for 2743-2744m depth interval

| PHI-N | PHI-D | PHIE | VSH-CP | VSH-GR | PHI-N | PHI-D | PHIE | VSH-CP | VSH-GR |
|---|---|---|---|---|---|---|---|---|---|
| 0.087 | 0.043 | 0.033 | 0.128 | 0.136 | 0.118 | 0.055 | 0.040 | 0.186 | 0.178 |
| 0.100 | 0.048 | 0.036 | 0.152 | 0.155 | 0.110 | 0.052 | 0.038 | 0.171 | 0.165 |
| 0.112 | 0.052 | 0.038 | 0.174 | 0.171 | 0.099 | 0.047 | 0.035 | 0.152 | 0.146 |
| 0.119 | 0.055 | 0.040 | 0.189 | 0.181 | 0.088 | 0.041 | 0.031 | 0.136 | 0.125 |
| 0.121 | 0.056 | 0.041 | 0.193 | 0.184 | 0.077 | 0.036 | 0.026 | 0.121 | 0.106 |

It is observed that shale volumes estimated from cross plots are in good agreement with gamma ray log which proves the accuracy of this approach for shale characterization in formation evaluation process (Figures 8 and 9 are presented as sample comparison plots). Integration of neutron-density cross-plot analysis for above depth intervals shows that shale distribution in the studied field is mainly dispersed with few of laminar shale and the main reason of low productivity of wells is pore throat plugging by dispersed clay minerals. Based on effective porosity values estimated, it is also observed that the reservoir quality decreases with increasing depth and the majority of gas production is from upper zones.

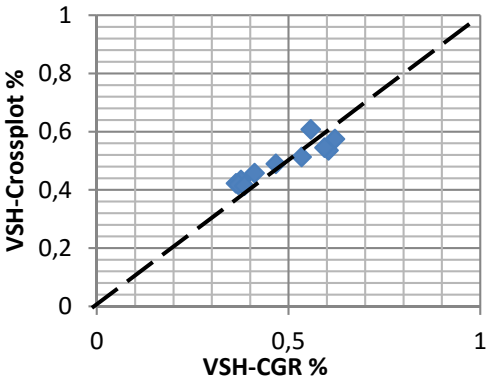


**Figure 8.** $V_{sh}$ from cross-plot Vs. $V_{sh}$ from gamma ray log for 2718.5-2719.5m depth interval

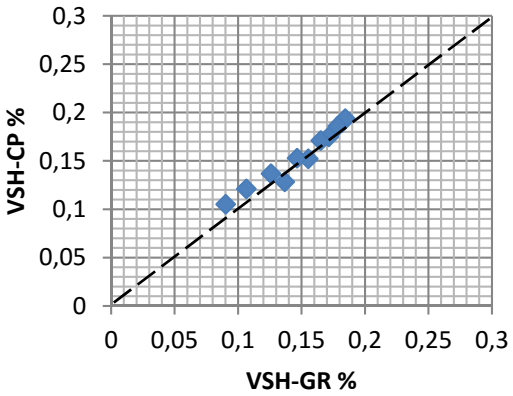


**Figure 9**. $V_{sh}$ from cross-plot method vs $V_{sh}$ from gamma ray log for 2743-2744 m depth interval

## 4. Conclusions

- The present work determines shale type, shale volume and effective porosity in one of Iranian gas fields by using triangle neutron-density porosity cross-plot approach.
- Shale distribution in the investigated formation is mainly dispersed with few of laminar ones. Based on estimated effective porosity values from cross-plot, one can conclude that the reservoir quality decreases with increasing depth.
- Estimated shale volumes from cross-plot are validated with gamma ray log (CGR) via stieber equation. Values of $\varphi_e$ are also compared to core analysis data. Good agreement of results shows that neutron-density cross-plot is a useful approach for determination of $V_{sh}$ and $\varphi_e$ from conventional log data.
- This method can be used for any formation but properties of shale layers (i.e. $\varphi_{NSh}$, $\varphi_{DSh}$) should be determined throughout the study area and be recalibrated as more wells drilled.

## References

[1] Brock, j., 1986. Applied open-hole log analysis. Gulf publishing company, Houston, Texas
[2] Mehana, M., El-monier, I., 2016. Shale characteristics impact on Nuclear Magnetic Resonance. Petroleum, In Press, doi: 10.1016/j.petlm.2016.02.002
[3] Kamel, M.H., Mohamed, M.M., 2006. Effective porosity determination in clean/shaly formations from acoustic logs. Journal of Petroleum Science and Engineering, 51(3-4): 267-274
[4] Ruhovets, N. Fertl, W. H., 1982. Volumes, Types, and Distribution of Clay Minerals in Reservoir Rocks Based on Well Logs. Pittsburgh, Pennsylvania, 64-79
[5] Abudeifa, A. M., Attiaa, M. M., Radwanb, A. E., 2016. Petrophysical and petrographic evaluation of Sidri Member of Belayim Formation, Badri field, Gulf of Suez, Egypt. Journal of African Earth Sciences, 115: 108-120
[6] Aquino-López, A., Mousatov, A., Markov, M., Kazatchenko, E., 2015. Modeling and inversion of elastic wave velocities and electrical. Journal of Applied Geophysics, 116: 28-42
[7] Worthington, P. F., 1985. The Evolution of Shaly-Sand Concepts in Reservoir Evaluation. The Log Analyst, 26(1): 23-40
[8] Ransom, R.C., 1977. Methods Based On Density and Neutron Well-logging Responses To Distinguish Characteristics Of Shaly Sandstone Reservoir Rock. The Log Analyst, 18(3): 47-66
[9] Ghorab, M., Ramadan, M. A., Nouh, A., 2008. The Relation between the Shale Origin (Source or non-Source) and its Type for Abu Roash Formation at Wadi El- Natrun Area, South of

Western Desert, Egypt. Australian Journal of Basic and Applied Sciences, 2(3): 360-371
[10] Tiab, D., Donaldson, E., 2004. Petrophysics: Theory and Practice of Measuring Reservoir Rock and Fluid Transport Properties. Second edition, Gulf Professional Publishing, Houston, Texas
[11] Fertl, W. H., 1981. Openhole Crossplot Concepts: A Powerful Technique in Well Log Analysis. Journal of Petroleum Technology, 33(3): 535-549
[12] Bigelow, E. l., 1992. Introduction to Wireline Log Analysis. Western Atlas International Inc., Houston, Texas
[13] Bassiouni, Z., 1994. Theory, measurement, and interpretation of well logs. Henry L. Doherty Memorial Fund of AIME, Society of Petroleum Engineers, Texas
[14] Wei, Y., Jianbo, W., Shuai, L., Kun, W., Yinan, Z., 2014. Logging identification of the Longmaxi mud shale reservoir in the Jiaoshiba. Natural Gas Industry, 1(2): 230-236
[15] Archie, G., 1942. The Electrical Resistivity Log as an Aid in Determining Some Reservoir Characteristics. Transactions of the AIME, 146(1): 54-62
[16] Kamel, M. H., Mabrouk, W. M., 2003. Estimation of shale volume using a combination of the three. Journal of Petroleum Science and Engineering, Volume 145, pp. 145-157
[17] Stieber, S., 1970. Pulsed Neutron Capture Log Evaluation - Louisiana Gulf Coast. Houston, Texas